NANO LETTERS

pubs.acs.org/NanoLett

# Bacterial Chemotaxis in Linear and Nonlinear Steady Microfluidic Gradients

**Tanvir Ahmed,[†] Thomas S. Shimizu,[‡] and Roman Stocker*,[†]**

[†]Ralph M. Parsons Laboratory, Department of Civil and Environmental Engineering, Massachusetts Institute of Technology, 77 Massachusetts Avenue, Cambridge, Massachusetts 02139 and [‡]FOM Institute for Atomic and Molecular Physics (AMOLF), Science Park 104, 1098 XG Amsterdam, The Netherlands

**ABSTRACT** Diffusion-based microfluidic devices can generate steady, arbitrarily shaped chemical gradients without requiring fluid flow and are ideal for studying chemotaxis of free-swimming cells such as bacteria. However, if microfluidic gradient generators are to be used to systematically study bacterial chemotaxis, it is critical to evaluate their performance with actual quantitative chemotaxis tests. We characterize and compare three diffusion-based gradient generators by confocal microscopy and numerical simulations, select an optimal design and apply it to chemotaxis experiments with *Escherichia coli* in both linear and nonlinear gradients. Comparison of the observed cell distribution along the gradients with predictions from an established mathematical model shows very good agreement, providing the first quantification of chemotaxis of free-swimming cells in steady nonlinear microfluidic gradients and opening the door to bacterial chemotaxis studies in gradients of arbitrary shape.

**KEYWORDS** Bacterial chemotaxis, microfluidics, gradient generator, hydrogel

Chemotaxis, the ability of cells to control their motile behavior in response to chemical signals, plays a major role in many microbial processes, from biofilm formation[1] to disease pathogenesis,[2] contaminant bioremediation,[3] and nutrient cycling in the ocean.[4−7] Considerable attention has been devoted to the fundamental mechanisms of chemotaxis in bacteria[8] and how the cellular response is governed by the spatiotemporal characteristics of chemical gradients.[9−13] The study of chemotaxis hinges strongly on the ability to expose cells to gradients that are quantifiable, controllable, and mimic those in natural environments.

A range of macroscopic approaches, including capillary assays[14] and stopped-flow diffusion chambers,[15] have revealed valuable information on bacterial chemotaxis. However, accurate control of gradients at cellular length scales is challenging in such macroscopic devices. In recent years a variety of microfluidic gradient generators have been proposed, leveraging the ability to accurately control fluid flow in the low Reynolds number regime to manipulate and quantify gradients with high accuracy at scales relevant to cells. Microfluidic gradient generators fall into two categories, flow-based and diffusion-based. The former can create steady gradients of arbitrary shape[16−19] to study chemotaxis of surface-attached cells, like breast cancer[18] and leukemia cells.[20,21] On the other hand, flow can be a strong confounding factor when studying free-swimming cells, because cells experience temporally varying gradients as they are transported by the flow[16,19] and flow-induced shear stresses can affect motility.[22]

In contrast, diffusion-based microdevices produce chemoeffector gradients without flow. Three approaches have been proposed, based on (i) stopping flow of two parallel streams, one containing chemoattractant,[23] (ii) maintaining a gradient in a quiescent fluid chamber by use of source and sink microchannels,[24] or (iii) maintaining a gradient across a hydrogel layer using source and sink microchannels.[25−28] The first approach produces unsteady gradients that only last minutes and is most suitable to study chemotaxis toward ephemeral chemical patches.[7,29,30] The second approach exposes cells to steady two-dimensional gradients and has been tested only qualitatively.[24] We focus on the third approach, hydrogel-based gradient generators, the most promising to study bacterial chemotaxis because of the flexibility in creating arbitrarily shaped gradients without flow.

Hydrogel-based gradient generators rely on the use of two parallel "feeder" microchannels (the "source" and "sink" channels), between which, a third "test" channel containing the cells is laid out (Figure 1). A constant flow rate is applied in the feeder channels, while there is no flow in the test channel. The source channel carries a solution of chemoeffector, while the sink channel typically carries buffer. The chemoeffector diffuses across the hydrogel from the source to the sink. This creates a steady concentration profile in the hydrogel, because the feeder channels provide constant-concentration boundary conditions. The characteristic time to set up the gradient, $T \sim L^2/(2D)$, is determined by the diffusion of the chemoeffector (of diffusivity $D$) across the distance $L$ between the feeder channels. Because the test channel is in direct contact with the hydrogel, its concentra-

* To whom correspondence should be addressed. E-mail: romans@mit.edu. Phone: 617 253 3726. Fax: 617 252 1458. Address: Massachusetts Institute of Technology, Building 48, Room 335, 15 Vassar Street, 02139 Cambridge MA. URL: web.mit.edu/romanstocker.

**Received for review: 04/6/2010**
**Published on Web: 07/29/2010**





DOI: 10.1021/nl101204e | *Nano Lett.* **2010,** *10,* 3379–3385

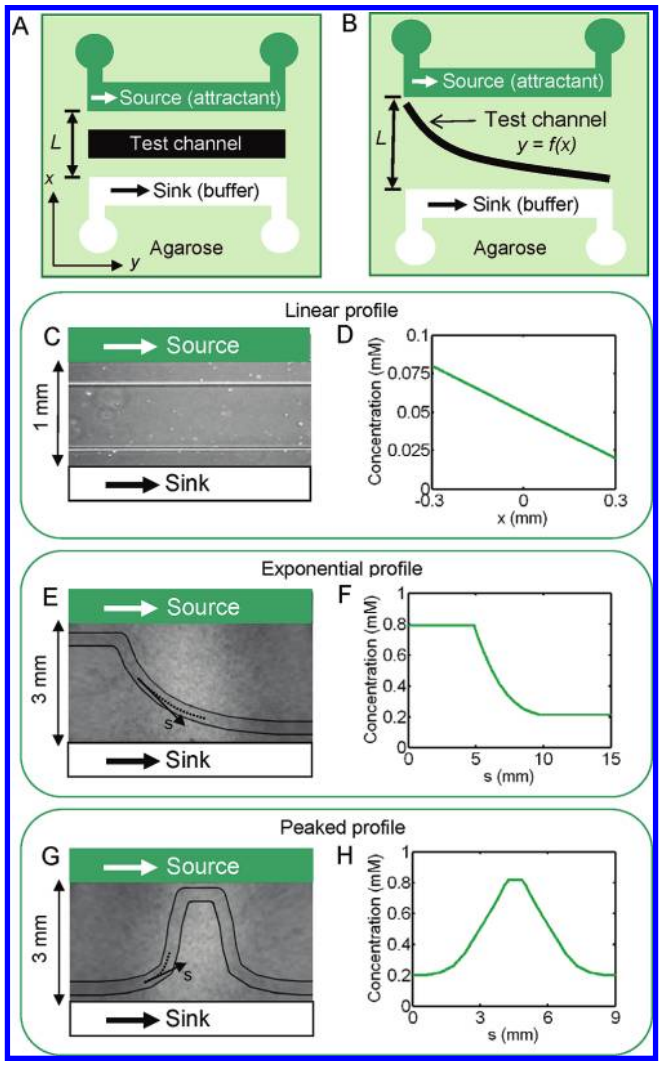


**FIGURE 1. (A,B) Schematic planar layouts of a class of diffusion-based microfluidic gradient generators for (A) linear and (B) nonlinear gradients. Constant-concentration boundary conditions in the source channel (flowing chemoattractant) and sink channel (flowing buffer) generate a steady gradient in the test channel by diffusion through the underlying agarose layer. *L* is the distance between the feeder channels (i.e., source and sink channels), measured between their inner walls facing toward the test channel. The direction of the gradient (*s*) corresponds to the *x*-axis in this case. (C,D) Microdevice to study chemotaxis in linear gradients. (C) Micrograph illustrating planar layout (source and sink channels are shown schematically in green and white, respectively) and (D) numerically computed concentration profile across the test channel for source and sink concentrations of 0.1 and 0 mM, respectively. (E−H) Microdevices to study chemotaxis in nonlinear gradients. (E,G) Micrographs showing the planar layout of the microdevices to create an exponential and a peaked concentration profile, respectively. *s* denotes the coordinate along the test channel. (F,H) Concentration profiles along the channels in E and G, respectively, computed numerically from the shape of the microchannels. The source and sink concentrations were 1 and 0 mM, respectively.**

tion profile reflects the concentration in the underlying hydrogel. This enables the generation of arbitrarily shaped gradients by appropriately configuring the planar layout of the test channel.[28] After the gradient is established in the hydrogel, cells are injected in the test channel. The gradient in the test channel is rapidly generated over a time scale $T_H \sim H^2/(2D)$, determined by the diffusion of the chemoeffector across the height $H$ of the test channel. For small molecules ($D = 5 \times 10^{-10}$ m$^2$ s$^{-1}$) diffusing across a 100 $\mu$m deep test channel, $T_H = 10$ s. A commonly used hydrogel is agarose (often at ~3% w/v), which is highly transparent in thin (~1−3 mm) layers, biocompatible, can be molded to form microchannels, and is quick and easy to assemble because of its thermal gelation properties.[27] The diffusivity of small molecules in agarose is the same as in water.[25]

Several implementations of hydrogel-based microfluidic gradient generators have been proposed. Channels can be fabricated in the hydrogel[25,26,31] or in a PDMS layer attached to a hydrogel slab.[28] The latter system has been used to generate arbitrarily shaped gradients by fabricating test channels with the appropriate planar layout[28] and has been tested for surface-attached cells.[32] These devices are extremely promising to study bacterial chemotaxis, yet their performance as chemotaxis assays has rarely been assessed quantitatively in terms of the bacterial response (but see refs 31 and 39) and to date no bacterial chemotaxis studies have been performed in steady, nonlinear microfluidic gradients. We compared three hydrogel-based gradient generators, selected an optimal design, and applied it to quantify the chemotactic response of *Escherichia coli* to linear and nonlinear chemoattractant gradients. To determine the applicability of these microdevices as chemotaxis assays, we used a relevant metric for chemotactic performance, the quantitative cell distribution along a chemical gradient, and compared it with predictions from a mathematical model.

We studied three configurations of a hydrogel-based gradient generator, having a 1 mm thick agarose layer sandwiched between a glass slide and a PDMS layer (Figure 1; Supporting Information, Methods). The microdevices used to generate steady linear gradients consisted of three parallel channels (Figure 1), each 600 $\mu$m wide. In design 1, all three channels were patterned in the PDMS layer (Figure 2A). In design 2, they were patterned in the agarose layer (Figure 2B). In design 3, the feeder channels were patterned in agarose and the test channel in PDMS (Figure 2C). Diffusion from the source (carrying a concentration $C_0$) to the sink (carrying a buffer solution) establishes a concentration gradient across the agarose. Common to all three designs, the flow-through configuration of the feeder channels eliminates the need for open-air reservoirs[28] and their periodic replenishment to maintain the gradient. When the feeder channels are far apart compared to the agarose thickness, the hydrogel domain is nearly one-dimensional and solution of the diffusion equation yields the linear concentration profile $C(x) = xC_0/L = xG_E$, where $G_E = C_0/L$ is the magnitude of the predicted one-dimensional gradient.

We used confocal laser scanning microscopy to measure $C(x)$ (Figure 3A−C; Supporting Information, Methods). Buffer was flowed at 1 $\mu$L/min in the feeder channels with addition of 100 $\mu$M fluorescein to the source channel. We waited 30



DOI: 10.1021/nl101204e | *Nano Lett.* **2010,** *10,* 3379–3385

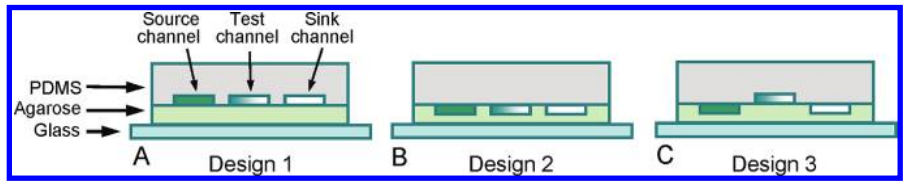


FIGURE 2. Schematic vertical cross sections of three different designs of the diffusion-based microfluidic gradient generator. The designs differ in the arrangement of the source, sink and test channels within the agarose and PDMS layers. (A) Design 1 with all three channels in the PDMS layer. (B) Design 2 with all three channels in the agarose layer. (C) Design 3 with source and sink channels in the agarose layer and test channel in the PDMS layer. In all designs, the test channel was separated from the feeder (i.e., source and sink) channels by a 200 $\mu$m wide layer of PDMS (A,C) or agarose (B), resulting in an edge-to-edge distance between the feeder channels of $L = 1$ mm. The intensity of the green shading is illustrative of the chemoattractant field in the channels (shown quantitatively in Figure 4).

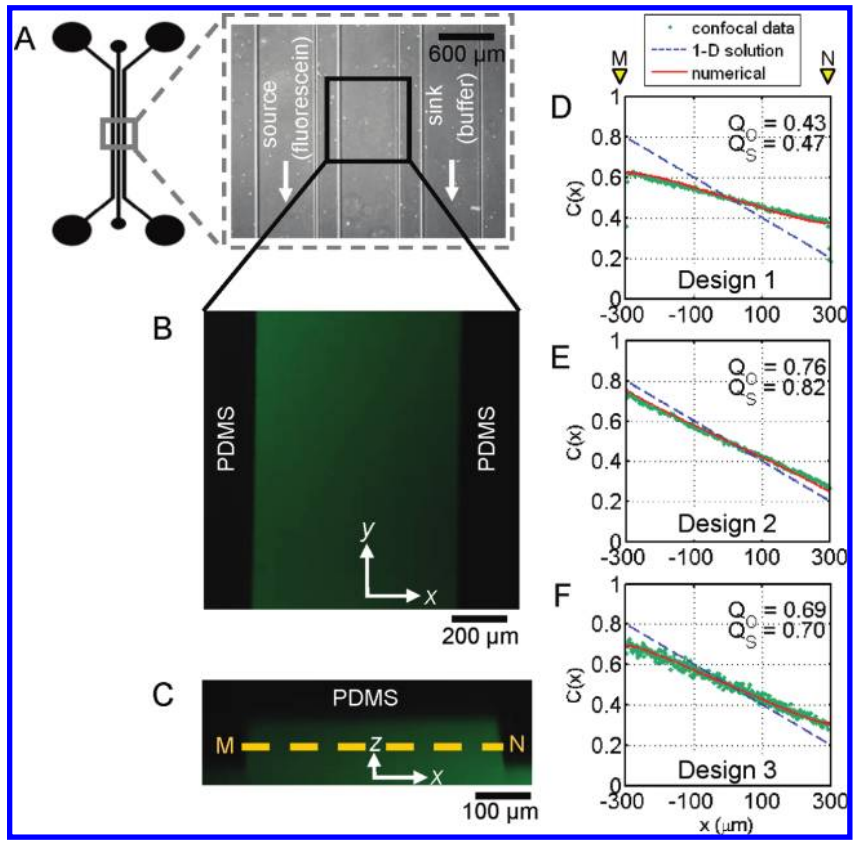


FIGURE 3. (A) Planar layout of the microdevice to generate a steady linear gradient (schematic and micrograph). (B) Confocal image showing fluorescence at mid-depth in the test channel for the planar section defined by the black box in A. One hundred micromolar fluorescein was added to the source channel (shown in A). (C) Vertical line-scan of the test channel taken along the centerline of the same region. The dashed line MN indicates mid-depth and corresponds to the image in B. (D−F) Concentration profiles across the width of the test channel at channel mid-depth for designs 1 (D), 2 (E), and 3 (F) (see Figure 2). The green dots are confocal data for fluorescence intensity, obtained along the mid-depth cross-section of each test channel (line MN in C). The red lines are numerically modeled profiles, taken along MN in Figure 4A−C, respectively. Triangular markers labeled M and N indicate the corresponding points in panel C and Figure 4A−C. The blue dashed line corresponds to the one-dimensional solution, that is, the profile predicted if concentration decayed linearly between source and sink. $Q_O$ measures the ratio of the magnitudes of the experimentally observed gradient and the predicted one-dimensional gradient. $Q_S$ measures the ratio of the magnitudes of the numerically computed gradient and the predicted one-dimensional gradient. $C(x)$ represents concentration normalized by the concentration in the source channel.

min after initiation of the feeder flows to allow the concentration field in the agarose to be established (for $L = 1$ mm this occurs over $T \sim L^2/(2D) = 17$ min). Then, buffer was injected in the test channel to mimic injection of a cell suspension and measurements started within minutes. Concentration profiles $C(x)$ recorded at channel mid-depth (Figure 3D−F, green dots) were highly linear. A linear least-squares fit to $C(x)$ within the test channel yielded the magnitude of the experimentally observed gradients, $G_O$, and confirmed the linearity of the gradients ($r^2 > 0.98$ for all three designs). Importantly, we found that $G_O$ was considerably lower than $G_E$ (Figure 3D−F, dashed blue line) and differed among the designs. The ratio of the magnitudes of the experimentally observed gradient and the predicted one-dimensional gradient, $Q_O = G_O/G_E$, was 0.43, 0.76, and 0.69 for designs 1, 2, and 3, respectively.



DOI: 10.1021/nl101204e | Nano Lett. 2010, 10, 3379–3385

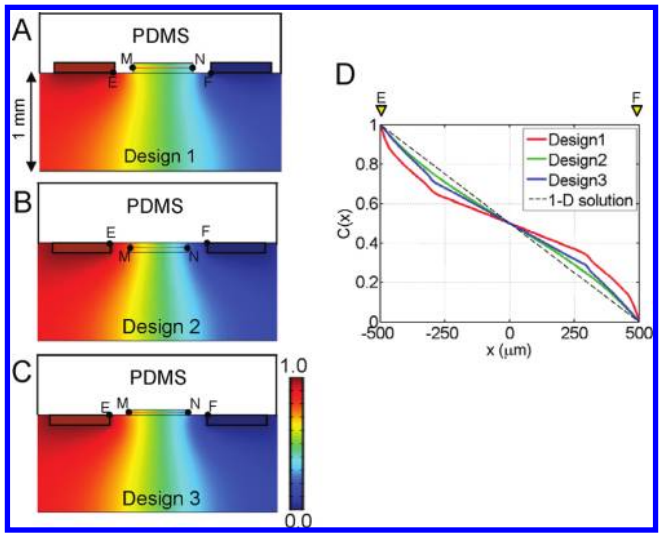


**FIGURE 4. (A−C) Numerically modeled concentration fields in the agarose layer and in the test channel (middle channel in each panel) for designs 1 (A), 2 (B), and 3 (C) (see Figure 2). Transects EF and MN indicate cross sections at the top of the agarose layer and at mid-depth in the test channel, respectively, and correspond to the numerically modeled concentration profiles plotted in panel D and in Figure 3D−F, respectively. (D) Numerically modeled concentration profiles, $C(x)$, at the top of the agarose layer, along lines EF in panels A−C. Triangular markers labeled E and F indicate the corresponding points in panels A−C. The dashed line is the one-dimensional solution, that is, the profile predicted if concentration decayed linearly between source ($x = -500$ $\mu$m) and sink ($x = 500$ $\mu$m). These profiles show that the concentration profile in the agarose layer is not linear and that the departure from linearity is design-dependent. In all cases, concentrations were normalized by the concentration in the source channel.**

Numerical simulations of the diffusion equation (Supporting Information, Methods) showed good agreement with measured profiles (Figure 3D−F, red line). Linear least-squares fitting of the simulated concentration profiles within the test channel yielded the magnitude of the numerically computed gradient, $G_S$, and confirmed that gradients were highly linear ($r^2 > 0.99$ for all three designs). The ratio of the magnitudes of the numerically computed gradient and the predicted one-dimensional gradient, $Q_S = G_S/G_E$, was 0.47, 0.83, and 0.70 for designs 1, 2, and 3, respectively, in close agreement with the observed ratios, $Q_O$. These results imply a steeper decay profile in the regions flanking the test channel, since the magnitude of the gradient averaged over the entire distance from the source channel to the sink channel must still be equal to $G_E$ to satisfy conservation of flux. This was confirmed by numerical simulations of $C(x)$ at the top of the agarose layer (Figure 4); while $C(x)$ is linear within the test channel, it is flanked by nonlinear regions where the magnitude of the gradient is greater than $G_E$. This nonlinearity is more pronounced in design 1, consistent with the lower value of $Q_O$ and $Q_S$.

These findings show that the magnitude of the chemoeffector gradient within the test channel will be less than $G_E$ (by up to 50%) and the geometry of the system must be accounted for in determining the actual gradient magnitude. This effect of geometry was not realized in previous studies based on wide-field fluorescence microscopy measurements.[25,26] The latter, however, is inappropriate for accurate characterization of the test-channel gradients because the out-of-plane fluorescence from the agarose layer, which is considerably thicker than the test channel, can override that of the test channel. This points to the importance of accurately quantifying the gradient through cross-sectional imaging and mathematical modeling.

This analysis leads us to select design 3 as the best choice for bacterial chemotaxis applications for two reasons. First, design 3 establishes a gradient whose magnitude is closer to $G_E$ compared to design 1. Second, design 3 enables the fabrication of more complex designs for the test channel compared to design 2, because patterning occurs in the PDMS as opposed to the agarose. Fabrication of deeper channels (~500 $\mu$m) was also found to be easier in PDMS than agarose, which tends to get torn when peeled off from the silicon master if thick. The chemotaxis experiments that follow will thus be based on the configuration in design 3.

We first performed chemotaxis experiments in linear concentration profiles, by exposing the bacteria *Escherichia coli* AW405 to gradients of α-methylaspartate, a nonmetabolizable analog of aspartate.[33] Gradients were created by flowing 0.1 or 1.0 mM α-methylaspartate in the source channel and buffer in the sink channel. After a time sufficient to reach a steady concentration field in the agarose (~17 min), a bacterial suspension was manually injected in the test channel by gentle pressure. Then, the inlet and outlet of the test channel were sealed, using drops of heated, liquid agarose or small PDMS blocks, to prevent residual flow in the channel and evaporation. Bacteria were filmed at channel mid-depth, using a computer-controlled inverted microscope equipped with a CCD camera. From movies we obtained both long-time-exposure images of the bacterial distribution and positions of individual bacteria. The latter were binned to yield the cell concentration profile along the gradient (Methods).

Flagellar rotation enables *E. coli* to swim and switching between clockwise and anticlockwise rotation results in tumbling (directional change) and smooth swimming, respectively. An increasing attractant concentration causes a suppression of tumbling[34] depending on the temporal change of attractant experienced by a swimming cell. The result is a net migration toward higher attractant concentrations.[11] In linear gradients, cells indeed accumulated near the edge of the test channel closest to the source channel (Figure 5A), resulting in a strongly skewed steady-state bacterial distribution (Figure 5B, bars).

To test the performance of the gradient generator in a chemotaxis assay, we compared the observed bacterial distribution with that predicted from a mathematical model (Supporting Information, Methods). The model computes the concentration field in the test channel, $C$, by solving the



DOI: 10.1021/nl101204e | *Nano Lett.* **2010,** *10,* 3379–3385

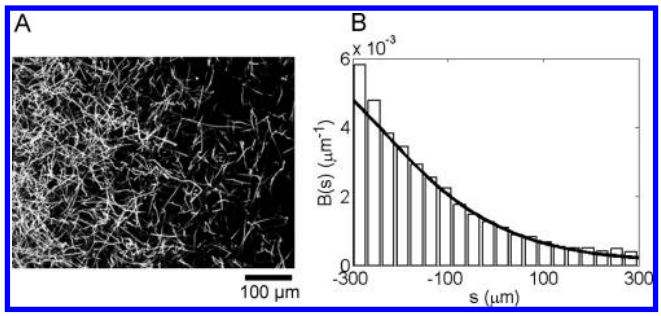


**FIGURE 5. Chemotactic response of the bacteria *E. coli* to a linear gradient of α-methylaspartate. A constant flow (1 μL/min) was maintained in the source and sink channels, containing 0.1 mM α-methylaspartate and motility buffer, respectively (see Figure 1C for the microdevice layout). This corresponds to a predicted one-dimensional gradient magnitude $G_E = 0.1$ mM/mm and an actual gradient magnitude $G_O = 0.069$ mM/mm (since $Q_O = 0.69$, see text). (A) Long-time-exposure image, recorded over 9.4 s, showing trajectories of *E. coli* cells. Note the accumulation of cells in the highest concentration region, on the side of the test channel closest to the source channel (left). (B) Normalized distribution of *E. coli* cells along the gradient, $B(s)$, from the experiments (bars) and the numerical model (line). The model result is the solution of the bacterial transport equation (eqs 1, 2) for $\mu = 5.9 \times 10^{-6}$ cm$^2$ s$^{-1}$ and $\chi_0 = 5.0 \times 10^{-4}$ cm$^2$ s$^{-1}$. $B(s)$ was normalized so as to have an area of 1.**

diffusion equation, and the distribution of cells, $B$, by solving the bacterial transport equation[11,12,35]

$$\frac{\partial B}{\partial t} = \frac{\partial}{\partial s}\left(\mu \frac{\partial B}{\partial s}\right) - \frac{\partial}{\partial s}(V_C B) \tag{1}$$

$$V_C = \frac{8V}{3\pi} \tanh\left(\frac{\chi_0 \pi}{8V} \frac{K_D}{(K_D + C)^2} \frac{dC}{ds}\right) \tag{2}$$

where $t$ is time, $s$ is the longitudinal coordinate along the microchannel (Figure 1), and $\mu$ is the random motility coefficient, measuring the diffusivity of a population of bacteria resulting from their random walk behavior.[13] The chemotactic velocity, $V_C$, represents the net drift velocity toward higher chemoattractant concentrations, $K_D$ is the receptor/ligand dissociation constant (= 0.125 mM[36]), $V$ is the two-dimensional swimming speed, and $\chi_0$ is the chemotactic sensitivity coefficient, measuring the strength of attraction of the cells to a given chemical. The bacterial transport equation has previously been used as a model to fit data from population-scale measurements to quantify the intensity of random motility and chemotaxis.[15,37]

For the linear gradient generator (Figure 1C), the direction of the gradient $s$ corresponds to $x$ and the chemoattractant concentration profile $C(x)$ is shown in Figure 1D. The observed bacterial distribution was strongly skewed toward higher chemoattractant concentrations (Figure 5B). Nonlinear $\chi$-square fitting and uncertainty analysis of the random motility and chemotaxis parameters, $\mu$ and $\chi_0$, with the observed bacterial distribution (Supporting Information) yielded $\mu = (5.9 \pm 0.7) \times 10^{-6}$ cm$^2$ s$^{-1}$ and $\chi_0 = (5.0 \pm 0.7) \times 10^{-4}$ cm$^2$ s$^{-1}$ (the error bounds represent 95% confidence intervals). The best-fit values provide an accurate description of the observed bacterial distribution (Figure 5B, solid line) and are in general agreement with recently reported values for chemotaxis of *E. coli* AW405 toward α-methyl-aspartate[12,38] ($\mu = (3.3-3.8) \times 10^{-6}$ cm$^2$ s$^{-1}$; $\chi_0 = (2.4-12.4) \times 10^{-4}$ cm$^2$ s$^{-1}$), particularly in view of the sensitivity of motiliy and chemotaxis to small changes in growth and experimental conditions.[10,15,38,39]

Fabrication of test channels with appropriate planar layouts enables the generation of steady, arbitrarily shaped gradients.[28] We investigated the response of *E. coli* to two types of nonlinear concentration profiles, an exponential profile connecting two constant-concentration regions (Figure 1E) and a peak in concentration (Figure 1G). In both cases, the distance $L$ between the feeder channels was 3 mm, resulting in a gradient setup time of $T = 2.5$ h. Although this design necessarily yields a finite gradient in the transverse direction across the channel, the gradient experienced by swimming cells is primarily in the longitudinal direction, parallel to the channel walls, because of the relatively narrow channel width (400 μm). The concentration gradient seen by the cells is therefore well approximated by d$C$/d$s$ (Figure 1E,G). If the shape of the microchannel's centerline is $y(x)$, the concentration profile and its gradient along the channel are[28] $C(s) = G_O \int (1 + y_x^2)^{-1/2}\, ds$, $dC/ds = G_O(1 + y_x^2)^{-1/2}$, where $y_x = dy/dx$. The distribution of *E. coli* cells was recorded 1 h after injection in the test channel, by rapidly translating the microscope stage along the channel and acquiring a movie at each of 15 (exponential profile) and 25 (peaked profile) positions.

In the exponential profile, bacteria migrated from the lower to the higher chemoattractant concentration, creating a peak in cell concentration followed by a depleted region (Figure 6A,B). The peak was positioned at the beginning of the constant, high-chemoattractant-concentration region. This distribution was compared with that predicted from the mathematical model (eqs 1 and 2) with good agreement in the location and magnitude of the peak and depleted regions (Figure 6B, solid line). The best fit, computed by nonlinear $\chi$-square fitting (Supporting Information), was obtained for $\mu = (7.0 \pm 0.5) \times 10^{-6}$ cm$^2$ s$^{-1}$ and $\chi_0 = (4.5 \pm 0.2) \times 10^{-4}$ cm$^2$ s$^{-1}$, consistent with the values obtained for the linear concentration profile at the 95% confidence level and with the literature ranges cited above. Observations of bacterial chemotaxis in exponential gradients are not new and have been performed before using macroscopic devices,[9,15] where gradients were created by capillary assays,[40] step addition,[9] or stopped flow.[15] However, in those approaches gradients were unsteady and concentration fields difficult to control and quantify.[15,37] Here we were able to observe the response of bacteria to a steady exponential chemoattractant gradient and successfully compared it with theoretical predictions.



DOI: 10.1021/nl101204e | *Nano Lett.* **2010,** *10,* 3379–3385

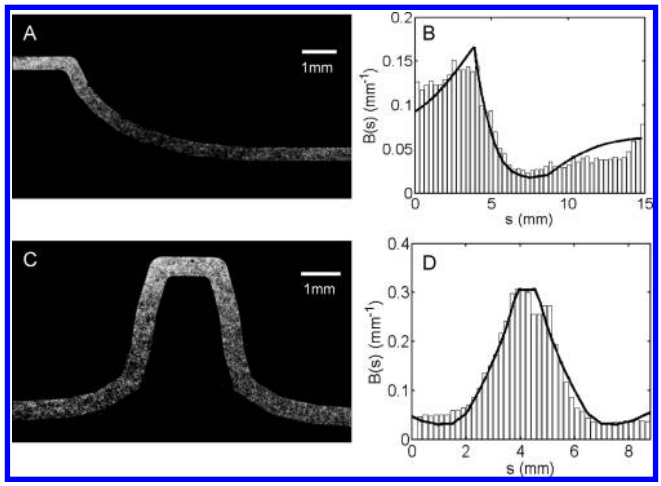


**FIGURE 6. Response of *E. coli* to (A,B) an exponential and (C,D) a peaked concentration profile of α-methylaspartate (see Figure 1E−H for the microdevices' layout). The concentration of α-methylaspartate in the source and sink channels was 1 and 0 mM, respectively. (A,C) Long-time-exposure images of cell trajectories, constructed from a mosaic of 7 (A) and 8 (C) images, each recorded over 6.7 s and acquired in rapid sequence. Accumulation of cells in the highest concentration region is evidenced by the high density of trajectories (white). (B,D) Normalized distribution of *E. coli* cells along the test channel, $B(s)$, from the experiments (bars) and the numerical model (solid line). The model results correspond to the solution of the bacterial transport equation (eqs 1 and 2) for the best-fit values of $\mu$ and $\chi_0$. (B) $\mu = 7.0 \times 10^{-6}$ cm$^2$ s$^{-1}$, $\chi_0 = 4.5 \times 10^{-4}$ cm$^2$ s$^{-1}$. (D) $\mu = 7.0 \times 10^{-6}$ cm$^2$ s$^{-1}$, $\chi_0 = 4.1 \times 10^{-4}$ cm$^2$ s$^{-1}$. $B(s)$ was normalized so as to have an area of 1.**

In the peaked profile, bacteria swam into the higher concentration region from both sides, resulting in strong accumulation (Figure 6C,D). The best fit was again obtained by nonlinear $\chi$-square fitting, yielding $\mu = (7.0 \pm 0.4) \times 10^{-6}$ cm$^2$ s$^{-1}$ and $\chi_0 = (4.1 \pm 0.2) \times 10^{-4}$ cm$^2$ s$^{-1}$ (Figure 6D, solid line), consistent with results reported above. Chemotaxis in peaked concentration profiles applies, for example, to foraging of aquatic microbes, because nutrients in aquatic environments are often released from point sources[5] and result in Gaussian-type patches. Chemotaxis toward such patches has been studied with microdevices,[7,29,30] limited to transient patches. In contrast, here we observed the response of bacteria to a steady patch, a useful model in the limit of slow patch diffusion (e.g., high molecular weight compounds) or fast motility.

By creating steady concentration profiles, we could study the chemotactic response dynamics without the chemoeffector gradient changing over time. The decoupling of the temporal scales of the evolution of the chemical signal and the bacterial response is a highly desirable feature for chemotaxis studies, allowing for a simpler test of the gradient sensitivity and increased reliability in the quantification of random-motility and chemotaxis parameters. Another application of steady gradients has been made in identifying the logarithmic sensing mechanism of *E. coli*.[31] Here we have studied chemotaxis in arbitrarily shaped one-dimensional gradients, and the proposed microdevices can easily be modified to achieve alternative steady configurations, including two-dimensional or competing gradients.[39] We therefore expect that this class of microdevices will find a broad range of applications.

In addition to steadiness, an important feature of the proposed gradient generators is the rapid establishment of the gradient within the test channel once the gradient in the agarose layer is formed. In other diffusion-based designs,[24,41] cells experience an ever-changing concentration field while the gradient develops in the test channel. In our device and related designs[25,28] there is a significant separation of time scales between gradient generation in the agarose layer ($\sim L^2/2D$) and in the test channel ($\sim H^2/2D$). Whereas the former must be established by horizontal diffusion across a few millimeters ($L$) over one to several hours, the latter only requires vertical diffusion over $\sim$100 $\mu$m ($H$) and thus forms in a few seconds. On the other hand, the time required to generate the gradient in the agarose can be a drawback in some applications. Flow-based microdevices can generate gradients more rapidly,[18,20,21] but they expose cells to shear stresses. A recent method succeeded in eliminating shear from a flow-based device[42] by translating the gradient to a static chamber through a porous layer and can possibly be adapted to create arbitrarily shaped nonlinear gradients.

In summary, we compared the observed distribution of *E. coli* with model predictions for both linear and nonlinear gradients and obtained very good agreement with published literature values. These results demonstrate the applicability of hydrogel-based microfluidic gradient generators to quantitative chemotaxis studies of free-swimming cells and their versatility in generating arbitrarily shaped gradients. While we have focused here on microbial behavior, these devices will be applicable to a broad range of problems, whenever rapid establishment of stable gradients in the absence of flow is desired. We hope that the simplicity of fabrication of the proposed design, along with its versatility to explore a wide range of chemical environments, will appeal to researchers in many fields and contribute to improve our understanding of microbial and cellular processes.

**Acknowledgment.** We would like to thank Marcos for assistance in the initial stages of the device development, H. Berg for his gift of *E. coli* AW405, D. Irimia for advice on microfabrication, and time at the Harvard Biolabs Imaging Center. T.A. was supported by a Martin Fellowship for sustainability. T.S.S. was supported by NWO/FOM. This work was also supported by a grant from the Hayashi fund, from MIT's MISTI program, by NIH Grant 1-R21-EB008844 and NSF Grant OCE-0744641-CAREER to R.S.

**Supporting Information Available.** Methods including bacterial strain and chemoattractant, design and microfabrication of gradient generators, device operation and data acquisition, a description of the mathematical model, and a description of the optimization and error analysis are available. This material is available free of charge via the Internet at http://pubs.acs.org.



DOI: 10.1021/nl101204e | *Nano Lett.* **2010,** *10,* 3379–3385

## REFERENCES AND NOTES


(1) Pratt, L. A.; Kolter, R. *Mol. Microbiol.* **1998**, *30* (2), 285–293.
(2) Ottemann, K. M.; Lowenthal, A. C. *Infect. Immun.* **2002**, *70* (4), 1984–1990.
(3) Lanning, L. M.; Ford, R. M. *Biotechnol. Bioeng.* **2002**, *78* (5), 556–566.
(4) Jackson, G. A. *Limnol. Oceanogr.* **1989**, *34* (3), 514–530.
(5) Azam, F.; Long, R. A. *Nature* **2001**, *414* (6863), 495–498.
(6) Blackburn, N.; Fenchel, T.; Mitchell, J. *Science* **1998**, *282* (5397), 2254–2256.
(7) Stocker, R.; Seymour, J. R.; Samadani, A.; Hunt, D. E.; Polz, M. F. *Proc. Natl. Acad. Sci. U.S.A.* **2008**, *105* (11), 4209–4214.
(8) Berg, H. C. *E.coli in motion*; Springer-Verlag: New York, 2003.
(9) Dahlquist, F.; Lovely, P.; Koshland, D. *Nature (London), New Biol.* **1972**, *236* (65), 120–123.
(10) Ford, R. M.; Phillips, B. R.; Quinn, J. A.; Lauffenburger, D. A. *Biotechnol. Bioeng.* **1991**, *37* (7), 647–660.
(11) Rivero, M. A.; Tranquillo, R. T.; Buettner, H. M.; Lauffenburger, D. A. *Chem. Eng. Sci.* **1989**, *44* (12), 2881–2897.
(12) Ahmed, T.; Stocker, R. *Biophys. J.* **2008**, *95* (9), 4481–4493.
(13) Berg, H. C. *Random Walks in Biology*; Princeton University Press: Princeton, NJ, 1983.
(14) Adler, J. *J. Gen. Microbiol.* **1973**, *74* (1), 77–91.
(15) Ford, R. M.; Lauffenburger, D. A. *Biotechnol. Bioeng.* **1991**, *37* (7), 661–672.
(16) Mao, H. B.; Cremer, P. S.; Manson, M. D. *Proc. Natl. Acad. Sci. U.S.A.* **2003**, *100* (9), 5449–5454.
(17) Jeon, N. L.; Baskaran, H.; Dertinger, S. K. W.; Whitesides, G. M.; Van de Water, L.; Toner, M. *Nat. Biotechnol.* **2002**, *20* (8), 826–830.
(18) Saadi, W.; Wang, S. J.; Lin, F.; Jeon, N. L. *Biomed. Microdevices* **2006**, *8* (2), 109–118.
(19) Englert, D. L.; Manson, M. D.; Jayaraman, A. *Appl. Environ. Microbiol.* **2009**, *75* (13), 4557–4564.
(20) Walker, G. M.; Sai, J. Q.; Richmond, A.; Stremler, M.; Chung, C. Y.; Wikswo, J. P. *Lab Chip* **2005**, *5* (6), 611–618.
(21) Irimia, D.; Toner, M. *Lab Chip* **2006**, *6* (3), 345–352.
(22) Locsei, J. T.; Pedley, T. J. *Bull. Math. Biol.* **2009**, *71* (5), 1089–1116.
(23) Seymour, J. R.; Ahmed, T.; Marcos; Stocker, R. *Limnol. Oceanogr.: Methods* **2008**, *6*, 477–488.
(24) Atencia, J.; Morrow, J.; Locascio, L. E. *Lab Chip* **2009**, *9* (18), 2707–2714.
(25) Cheng, S. Y.; Heilman, S.; Wasserman, M.; Archer, S.; Shuler, M. L.; Wu, M. M. *Lab Chip* **2007**, *7* (6), 763–769.
(26) Diao, J. P.; Young, L.; Kim, S.; Fogarty, E. A.; Heilman, S. M.; Zhou, P.; Shuler, M. L.; Wu, M. M.; DeLisa, M. P. *Lab Chip* **2006**, *6* (3), 381–388.
(27) Haessler, U.; Kalinin, Y.; Swartz, M. A.; Wu, M. *Biomed Microdevices* **2009**, *11* (4), 827–35.
(28) Wu, H. K.; Huang, B.; Zare, R. N. *J. Am. Chem. Soc.* **2006**, *128* (13), 4194–4195.
(29) Seymour, J. R.; Ahmed, T.; Stocker, R. *J. Plankton Res.* **2009**, *31* (12), 1557–1561.
(30) Seymour, J. R.; Marcos; Stocker, R. *Am. Nat.* **2009**, *173* (1), E15–E29.
(31) Kalinin, Y. V.; Jiang, L. L.; Tu, Y. H.; Wu, M. M. *Biophys. J.* **2009**, *96* (6), 2439–2448.
(32) Abhyankar, V. V.; Toepke, M. W.; Cortesio, C. L.; Lokuta, M. A.; Huttenlocher, A.; Beebe, D. J. *Lab Chip* **2008**, *8* (9), 1507–1515.
(33) Adler, J. *Science* **1969**, *166* (3913), 1588–1597.
(34) Brown, D. A.; Berg, H. C. *Proc. Natl. Acad. Sci. U.S.A.* **1974**, *71* (4), 1388–1392.
(35) Chen, K. C.; Ford, R. M.; Cummings, P. T. *Siam J. Appl. Math.* **1998**, *59* (1), 35–57.
(36) Mesibov, R.; Ordal, G. W.; Adler, J. *J. Gen. Physiol.* **1973**, *62* (2), 203–223.
(37) Marx, R. B.; Aitken, M. D. *Appl. Environ. Microbiol.* **1999**, *65* (7), 2847–2852.
(38) Lewus, P.; Ford, R. M. *Biotechnol. Bioeng.* **2001**, *75* (3), 292–304.
(39) Kalinin, Y.; Neumann, S.; Sourjik, V.; Wu, M. M. *J. Bacteriol.* **2010**, *192* (7), 1796–1800.
(40) Adler, J.; Hazelbau.Gl; Dahl, M. M. *J. Bacteriol.* **1973**, *115* (3), 824–847.
(41) Saadi, W.; Rhee, S. W.; Lin, F.; Vahidi, B.; Chung, B. G.; Jeon, N. L. *Biomed. Microdevices* **2007**, *9* (5), 627–635.
(42) Kim, T.; Pinelis, M.; Maharbiz, M. M. *Biomed. Microdevices* **2009**, *11* (1), 65–73.




DOI: 10.1021/nl101204e | *Nano Lett.* **2010,** *10,* 3379–-3385